Imbalance of Mitochondrial Respiratory Chain Complexes in the Epidermis Induces Severe Skin Inflammation

Daniela Weiland, Bent Brachvogel, Johannes F.G. Neuhaus, Hue-Tran Hornig-Do, Johannes F G Neuhaus, Tatjana Holzer, Desmond J. Tobin, Carien M Niessen, Rudolf J Wiesner, Olivier Baris

Imbalance of Mitochondrial Respiratory Chain Complexes in the Epidermis Induces Severe Skin Inflammation

Daniela Weiland[1], Bent Brachvogel[2,3], Hue-Tran Hornig-Do[1], Johannes F.G. Neuhaus[1], Tatjana Holzer[3], Desmond J. Tobin[4], Carien M. Niessen[5,6,7], Rudolf J. Wiesner[1,5,6] and Olivier R. Baris[1]

Accumulation of large-scale mitochondrial DNA (mtDNA) deletions and chronic, subclinical inflammation are concomitant during skin aging, thus raising the question of a causal link. To approach this, we generated mice expressing a mutant mitochondrial helicase (K320E-TWINKLE) in the epidermis to accelerate the accumulation of mtDNA deletions in this skin compartment. Mice displayed low amounts of large-scale deletions and a dramatic depletion of mtDNA in the epidermis and showed macroscopic signs of severe skin inflammation. The mtDNA alterations led to an imbalanced stoichiometry of mitochondrial respiratory chain complexes, inducing a unique combination of cytokine expression, causing a severe inflammatory phenotype, with massive immune cell infiltrates already before birth. Altogether, these data unraveled a previously unknown link between an imbalanced stoichiometry of the mitochondrial respiratory chain complexes and skin inflammation and suggest that severe respiratory chain dysfunction, as observed in few cells leading to a mosaic in aged tissues, might be involved in the development of chronic subclinical inflammation.

Journal of Investigative Dermatology (2018) **138,** 132–140; doi:10.1016/j.jid.2017.08.019

INTRODUCTION

Skin aging is characterized by progressive structural and morphological changes, ultimately leading to functional alterations and higher susceptibility to developing diseases, ranging from common skin lesions to cancer (reviewed in Zouboulis and Makrantonaki, 2011). Therefore, identifying the molecular pathways involved appears crucial in order to develop therapeutic ways to reduce the incidence of such diseases in our society with steadily increasing life expectancy.

One hallmark of tissue aging, including skin, is chronic subclinical inflammation, also termed *inflammaging* (Franceschi et al., 2017). Recent in vivo experiments suggest that chronic and systemic inflammation is not only observed during aging but also accelerates this process (Jurk et al., 2014), and its involvement in many age-related diseases such as arthritis, atherosclerosis, cancer, diabetes, or neurodegeneration is now well established (reviewed in Zhuang and Lyga, 2014). Inflammaging is thought to originate from multiple intracellular sources including redox imbalance, oxidative stress, protein aggregates, or changes in membrane lipid composition, which ultimately lead to the secretion of proinflammatory cytokines (reviewed in Ponnappan and Ponnappan, 2011), but the fundamental mechanisms involved are not yet fully understood.

Aged skin is also characterized by the accumulation of deletions of mitochondrial DNA (mtDNA) (Eshaghian et al., 2006). This small, circular genome, which is present in hundreds of copies in every cell, codes for 13 crucial subunits of the mitochondrial respiratory chain (RC) as well as ribosomal and transfer RNA needed for translation inside the organelle. Consequently, large deletions will dramatically impair the balanced synthesis of the RC, thus altering many important cellular functions as soon as the load of deleted copies surpasses a critical threshold. Those cells with defective mitochondria, embedded among many normal cells for which the threshold has not been surpassed, give rise to the well-described mosaic pattern of mitochondrial deficiency observed in many tissues in elderly individuals (reviewed in Larsson, 2010). In the skin, mtDNA deletions are thought to result primarily from photo-aging (Berneburg et al., 1999; Birch-Machin et al., 1998) and can be found in both epidermis and dermis (Krishnan et al., 2004; Ray et al., 2000).

Because chronic inflammation and accumulation of mtDNA deletions are concomitant during skin aging, a causal link between both phenomena is possible. In recent years, material released from damaged mitochondria-like mtDNA, N-formylated peptides, mitochondrial RNAs, or the inner membrane lipid cardiolipin have been repeatedly postulated to act as damage-associated molecular patterns (Galluzzi et al., 2012; Iyer et al., 2013; van der Burgh and Boes, 2015). Moreover, the presence of mtDNA deletions at sites of inflammation has

[1]*Center for Physiology and Pathophysiology, Institute of Vegetative Physiology, University of Köln, Köln, Germany;* [2]*Department of Pediatrics and Adolescent Medicine, Experimental Neonatology, Medical Faculty, University of Köln, Köln, Germany;* [3]*Center for Biochemistry, Medical Faculty, University of Köln, Köln, Germany;* [4]*Centre for Skin Sciences, School of Life Sciences, University of Bradford, Bradford, UK;* [5]*Center for Molecular Medicine Cologne (CMMC), University of Köln, Köln, Germany;* [6]*Cologne Excellence Cluster on Cellular Stress Responses in Aging-Associated Diseases (CECAD), Köln, Germany; and* [7]*Department of Dermatology, University of Köln, Köln, Germany*

Correspondence: Rudolf J. Wiesner, Center for Physiology and Pathophysiology, Institute of Vegetative Physiology, Robert-Koch-Strasse 39, Köln 50931, Germany. E-mail: rudolf.wiesner@uni-koeln.de

Abbreviations: mtDNA, mitochondrial DNA; RC, respiratory chain; ROS, reactive oxygen species

Received 13 July 2017; revised 16 August 2017; accepted 16 August 2017; accepted manuscript published online 1 September 2017; corrected proof published online 14 November 2017

been reported in different tissues (Rygiel et al., 2015; Volmering et al., 2016), but it is not clear whether these deletions are the cause or consequence of inflammation.

To investigate whether the accumulation of mtDNA deletions and the ensuing mitochondrial dysfunction can lead to skin inflammation, we generated mice that express a dominant negative form of the mitochondrial helicase TWINKLE (Spelbrink et al., 2001) specifically in the epidermis (K320E-Twinkle^{Epi} mice). Patients harboring this mutation in the twinkle gene (gene name: *PEO1*) (Hudson et al., 2005) accumulate mtDNA deletions in many tissues, but because of their systemic disorder with severe neurological symptoms (sensory ataxic neuropathy with dysarthria and ophthalmoplegia [i.e., SANDO]), the presence of such deletions in their skin has not been studied.

RESULTS

K320E-Twinkle^{Epi} mice are short-lived but show macroscopic signs of skin inflammation

Genotyping (Figure 1a) showed that K320E-Twinkle^{Epi} mice were born at expected Mendelian ratios. Fluorescence of GFP, cloned downstream and serving as a surrogate for K320E-TWINKLE expression, was observed in the skin of mutant mice under UV light and was restricted to epidermis (Figure 1b). K320E-Twinkle^{Epi} mice appeared normal at birth but rapidly showed signs of growth retardation (Figure 1c and d) and usually died between postnatal days 5 and 8. Decreased blood glucose (GlucoMen LX assay; Menarini Diagnostics, Winnersh-Wokingham, UK) and increased lactate levels (Accutrend Plus assay; Roche Diagnostics, Basel, Switzerland), due to mitochondrial dysfunction in the large epidermal compartment, suggest that lactic acidosis is the most probable cause of death (Figure 1e and f). K320E-Twinkle^{Epi} mice consistently developed serous scabs at the ventral skin region and at the limb joints 2–3 days after birth (Figure 1g). Thus, although the early lethality of the mutant mice precluded any long-term aging study, these clear macroscopic signs of skin inflammation prompted us to further explore the link between expression of K320E-TWINKLE in epidermis and the inflammatory phenotype.

K320E-Twinkle^{Epi} mice show severe mtDNA depletion in the epidermis and few deletions

A massive reduction of mtDNA was observed in mutant epidermis (control = 1.00 ± 0.14, K320E-Twinkle^{Epi} = 0.09 ± 0.01) (Figure 2a) at birth, probably attributable to the combination of the severely impaired mtDNA processing activity of the mutated helicase (Goffart et al., 2009) and the high proliferation rate of keratinocytes. Large deleted mtDNA species were detected only by a nested, long-range PCR approach, which shows that their amounts were low (see Supplementary Figure S1a online). This suggests that deletions were either generated at a low rate or selected against by cellular quality control mechanisms involved in maintenance of mtDNA integrity, such as mitochondrial fusion/fission cycles (Chen et al., 2010) and autophagy/mitophagy (Dai et al., 2014).

Levels of electron transport chain protein complexes are differentially altered in the epidermis of K320E-Twinkle^{Epi} mice

K320E-Twinkle^{Epi} epidermal sheets showed reduced steady state levels of the index subunits NDUFA9 and UQCR2, representative for assembled complex I and III, respectively, whereas the mtDNA-encoded MTCO1 protein, representative of complex IV, was barely detectable (Figure 2b). In contrast, SDHB of complex II, which is entirely nuclear encoded, and the nuclear-encoded ATP5A subunit as part of a partially assembled ATP synthase (Hornig-Do et al., 2012), showed normal levels (Figure 2b). Therefore, the stoichiometry of assembled complexes of the RC is disturbed in mutant epidermis. This is in stark contrast to our previously published epidermal *Tfam* knockout mouse model (*Tfam*^{EKO}), which also shows a depletion of mtDNA but displays a complete absence of complexes I, III, and IV (Baris et al., 2011) (see Supplementary Figure S1b). In addition, Blue Native PAGE showed that the levels of the fully assembled complexes I, III, and IV were dramatically reduced in K320E-Twinkle^{Epi} epidermis, but those of complex II were again unaffected (Figure 2c). The proper assembly of these complexes was not impaired, because long exposure times showed the presence of the same assembly intermediates in mutants and controls (see Supplementary Figure S2 online). Altogether, these results show that the expression of K320E-TWINKLE severely disturbs the stoichiometry of the RC complexes in the epidermis without affecting their assembly from the existing pools of still synthesized subunits.

Epidermis of K320E-Twinkle^{Epi} mice shows impaired respiratory activity but normal mitochondrial mass

A COX (complex IV)/succinate dehydrogenase (complex II) double staining method was used to determine the onset of RC dysfunction. Loss of COX activity was already observed at embryonic day (E) 17.5 in K320E-Twinkle^{Epi} mice, indicated by blue succinate dehydrogenase staining in keratin 14-Cre–expressing epidermal cells and persisted after birth (Figure 2d). As expected, dermal fibroblasts of these animals displayed normal COX activity, showing again the specificity of our genetic approach. Flow cytometry using Mito Tracker Deep Red showed no variation of mitochondrial mass in isolated mutant keratinocytes (control = 26.54 ± 1.69, K320E-Twinkle^{Epi} = 32.33 ± 1.80; nonsignificant) (Figure 2e). In addition, expression of genes involved in mitochondrial biogenesis and mtDNA maintenance (*Nrf1, Pgc1a, Polg, Polg2, Polrmt, Tfam, Tfb1m, Tfb2m*) was similar, with the exception of twinkle (gene name: *Peo1*), which was overexpressed 5-fold in K320E-Twinkle^{Epi} mice, as expected (Figure 2f, and see Supplementary Table S1 online). Moreover, genes involved in mitochondrial dynamics (*Drp1, Fis1, Mfn1, Mfn2, Opa1*) or quality control (*Afg3l2, Clpp, Hsp60, Lonp1, mt-Hsp70, Oma1, Park2, Pink1*) had also normal expression levels, and staining of epidermal sections for TOM20 (20 kDa), an abundant protein of the import machinery of the organelle, showed no abnormalities in mitochondrial distribution (Figure 2g). Thus, the mitochondrial dysfunction observed in epidermis of K320E-Twinkle^{Epi} mice is not caused by a decrease in total mitochondrial mass, but by the disturbed stoichiometry and partial absence of RC complexes.

K320E-Twinkle^{Epi} mice exhibit abnormal epidermal differentiation and delayed barrier formation at the ventral region

Because scabs mainly developed at ventral skin, we investigated whether epidermal differentiation and skin structure

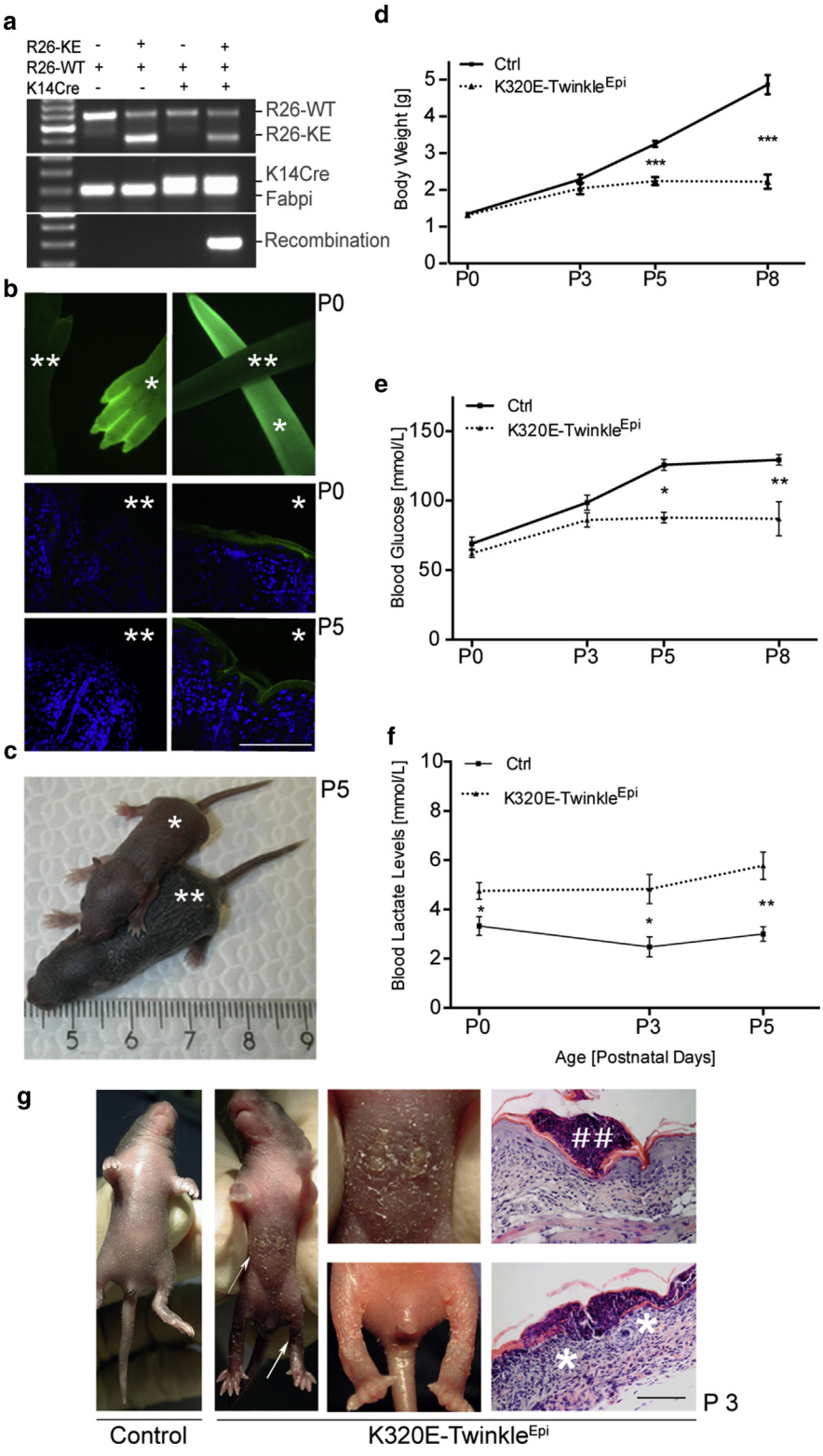

Figure 1. Growth retardation and early lethality of K320E-Twinkle^{Epi} mice. (**a**) PCR genotyping. (**b**) GFP expression in the epidermis of K320E-Twinkle^{Epi} mice at P0 and P5. *K320E-Twinkle^{Epi}, **control. The two upper panels show live animals under UV light; the four lower panels show cryosections counterstained with DAPI. Scale bar = 100 μm. (**c**) Macroscopic view of K320E-Twinkle^{Epi} and control mice at P5. (**d**) Reduced body weight and (**e**) blood glucose levels in mutants after birth. (**f**) Increased blood lactate levels in mutants. n = 3−15 per measured point, mean ± standard deviation. *$P < 0.05$, **$P < 0.01$, ***$P < 0.001$. (**g**) Left panels show serous scabs at the ventral skin and limb joints, visible at P3 in mutants. Right panels show disturbed skin architecture around the scabs (##) with granulation tissue (*). Ctrl, control; Fabpi, internal control; K14, keratin 14; KE, K320E-Twinkle; P, postnatal day; R26, Rosa-26-locus; WT, wild type.

were altered in this region. High resolution light microscopy and hematoxylin/eosin staining indeed showed disturbed ventral skin architecture, evidenced by epidermal dysplasia and enlarged keratinocytes with a tendency toward parakeratosis (Figure 3b and c). Moreover, immunofluorescence staining for keratin 14 (stratum basale), keratin 10 (stratum spinosum), and loricrin (stratum corneum) showed an irregular architecture of epidermal layers, despite normal expression of epidermal differentiation marker genes (Figure 3a, and see Supplementary Figure S3d online). Proliferation of basal keratinocytes was significantly increased at the scab area (Ki-67 positive cells: controls = 20 ± 2 per visual field; mutants = 29 ± 1 per visual field) (Figure 3d), which explains the observed thickening of the interfollicular

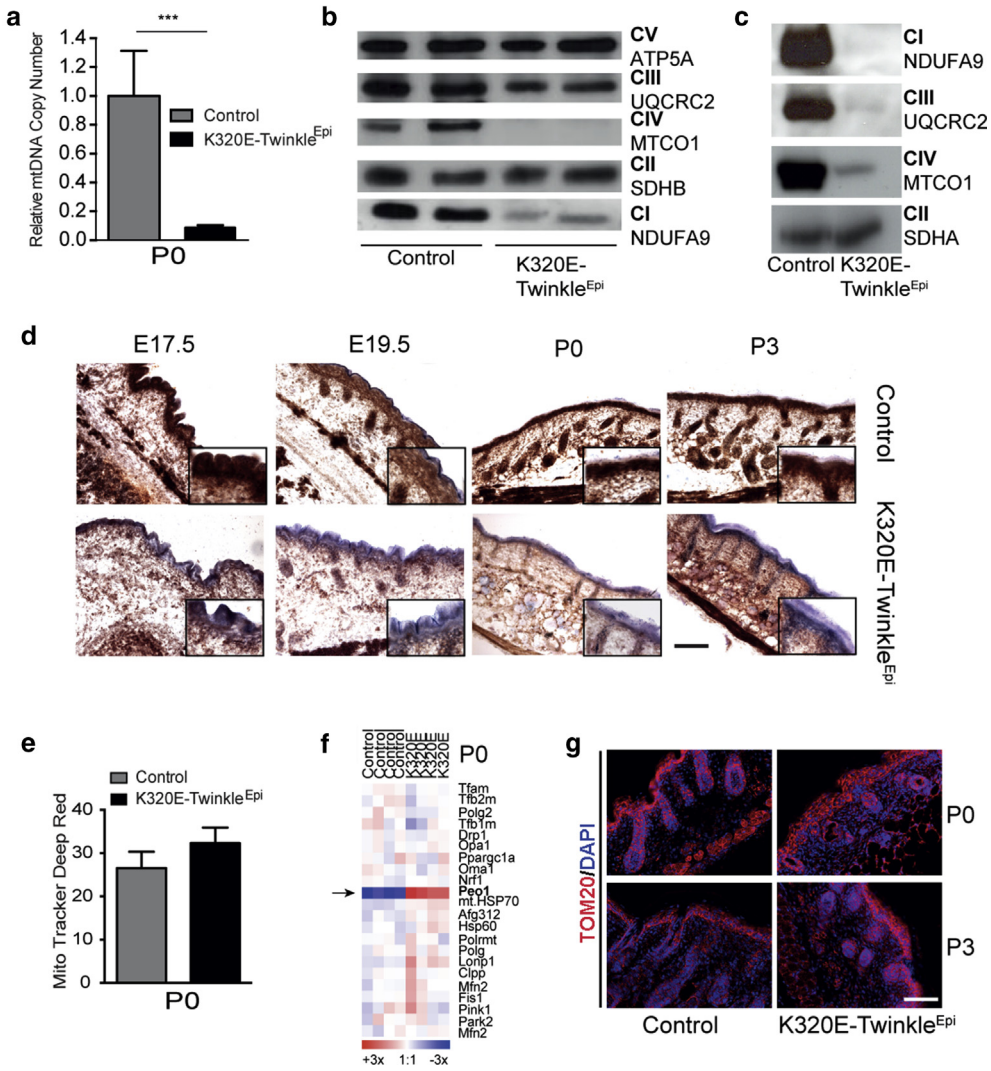

Figure 2. mtDNA depletion and impaired mitochondrial function in the epidermis of K320E-Twinkle^{Epi} mice. (**a**) Massive depletion of mtDNA copy number in K320E-Twinkle^{Epi} mice at P0 (quantitative PCR). n = 5, mean ± standard deviation. ***$P <$ 0.001, Student *t* test for unpaired samples. (**b**) Immunoblot of epidermal sheets and (**c**) Blue Native PAGE of isolated newborn keratinocytes showed a disturbed stoichiometry of the respiratory chain complexes I (CI) to V (CV). (**d**) COX-SDH enzymatic reaction showed respiratory chain dysfunction in the epidermis already in utero, as indicated by a blue color. Scale bar = 100 μm. (**e**) Flow cytometry showed no changes in mitochondrial mass using Mito Tracker Deep Red staining. (**f**) No differences in transcript levels of genes involved in mitochondrial biogenesis, mtDNA maintenance, and mitochondrial dynamics, except for twinkle (*Peo1*). (**g**) Normal distribution of mitochondria in mutant mice. Red indicates TOM20; blue indicates DAPI. Scale bar = 50 μm. E, embryonic day; mtDNA, mitochondrial DNA; P, postnatal day; SDH, succinate dehydrogenase.

epidermis (controls = 13.0 ± 1.0 μm, mutants = 23.8 ± 2.6 μm) (Figure 3e). This hyperproliferative status, notably in the absence of a functioning RC, was further emphasized by the increased expression of several genes involved in keratinocyte proliferation and skin regeneration (Figure 3f, and see Supplementary Table S1), such as *Areg* (fold change: +2.7), *Ereg* (+1.7), *Epgn* (+6.8), *Krt6a* (+3.5), *Krt6b* (+2.7), and *Krt16* (+2.0). In contrast, back skin showed a mostly normal architecture of epidermal layers (see Supplementary Figure S3a–c), but hair follicle development was severely altered, like in the ventral skin. This was evidenced by a reduced number of hair follicles, increased apoptosis, disturbed morphology, and decreased expression of genes for those keratin isoforms and keratin-associated proteins that are highly active in cells involved in hair formation (see Supplementary Figure S4 online and Supplementary Table S1). This further confirms previous results on the importance of mitochondrial RC function for hair follicle development (Hamanaka et al., 2013; Kloepper et al., 2015).

K320E-Twinkle^{Epi} mice display severe skin inflammation

The development of scabs at the ventral region at around postnatal days 2–3 was preceded by a massive infiltration of immune cells (Figure 4a–c), including macrophages and neutrophil granulocytes, which were recruited to this region already before birth at E17.5 or E19.5, respectively. At birth, expression of many cytokines and mediators of an immune response was increased in epidermis (Figure 4d), such as *Il1b* (fold change: +1.6), *Il24* (+2.7), and *Il33* (+2.0), but also the members of the tumor necrosis factor receptor superfamily *Tnfrsf1a* (+1.6), *Tnfrsf12a* (+1.6), and *Tnfrsf23* (+2.0), members of the S100 family, and the antimicrobial polypeptides *Tslp* (+1.6) and *Slpi* (+5.4), among others (see Supplementary Table S1).

To search for the initial cause for inflammation, we first asked if mitochondrial reactive oxygen species (ROS) production was increased because of the disturbed stoichiometry of the RC complexes. However, flow cytometry showed no changes of superoxide production in freshly isolated mutant keratinocytes (control = 179.6 ± 60.6; K320E-Twinkle^{Epi} = 133.3 ± 27.8) (Figure 5a). Also, there was no up-regulation of genes involved in antioxidant defense like *Cat, Sod1–3,* or *Gpx1–7* (Figure 5b), which would be the default response to increased ROS levels. Nevertheless, as expected, the severe mitochondrial dysfunction (Figure 2b–d) caused a significant decrease of the mitochondrial inner membrane potential

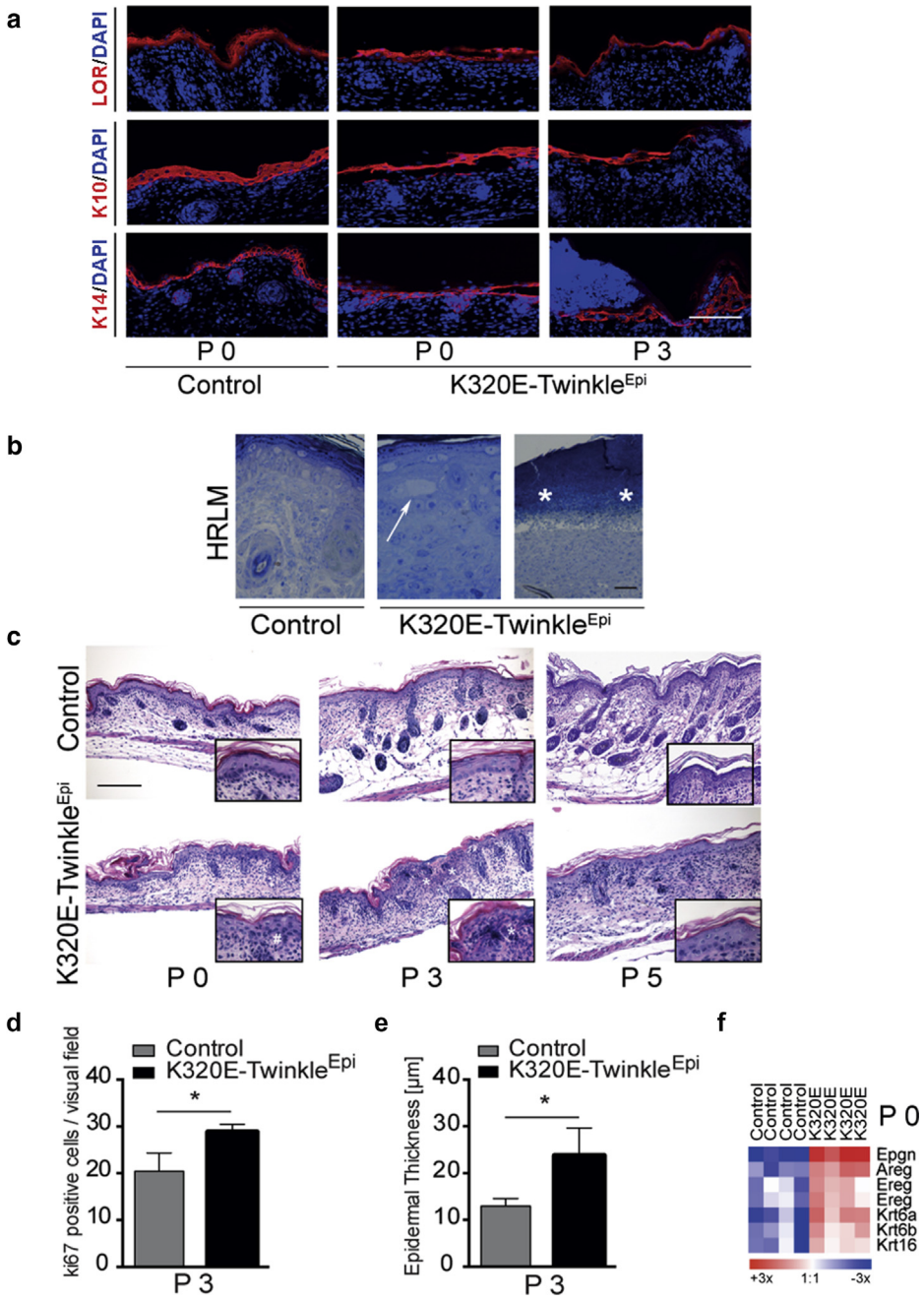

Figure 3. Abnormal differentiation in the ventral skin of K320E-Twinkle^{Epi} mice. (**a**) Irregular architecture of the different epidermal layers. Red indicates all markers; blue indicates DAPI. Scale bars = 100 µm. (**b**) High resolution light microscopy and (**c**) Hematoxylin/eosin stainings showed disturbed skin architecture with epidermal dysplasia, enlarged keratinocytes, vacuolation and rare hair follicle development in K320E-Twinkle^{Epi} mice. White arrow indicates vacuolation; white asterisks indicate granulation tissue. Scale bar = 20 µm for high resolution light microscopy and 100 µm for HE. (**d**) Significantly increased amount of proliferative (Ki-67^{+}) keratinocytes leading to (**e**) a thickening of the interfollicular epidermis at P3. n = 3 control, n = 5 K320E-Twinkle^{Epi}; mean ± standard deviation. *$P < 0.05$. (**f**) Increased expression of genes involved in keratinocyte proliferation and regeneration. K10, keratin 10; K14, keratin 14; lor, loricrin; P, postnatal day.

(Figure 5c), which matches with the fact that mutant keratinocytes do not produce more ROS (Figure 5a).

We then asked whether the observed inflammation could stem from developmental defects in ventral skin and disturbed barrier formation as previously described (Huebner et al., 2012). At birth, epidermis was impermeable to toluidine blue in both mutant and control mice (Figure 5d), but transcriptome data showed an increased expression of genes encoding small prolin-rich proteins and late cornified envelope proteins (Figure 5e, and see Supplementary Table S1). Because this suggested a compensatory response to a defective barrier in utero (Koch et al., 2000), we investigated earlier time points and could indeed observe a transient delay in barrier closure at E17.5 (Figure 5f). However, an even more severe delay in barrier closure was observed in *Tfam^{EKO}* animals at the same embryonic stage (see Supplementary Figure S5a online), which, on the other hand, never showed any signs of inflammation (see Supplementary Figure S5b), excluding the explanation that amniotic fluid alone (Huebner et al., 2012) has activated this severe inflammatory response.

DISCUSSION

To our knowledge, in this study we report a previously unknown link between an imbalanced RC in the epidermis and skin inflammation. Our data show that mtDNA depletion alone can be excluded as being responsible for the observed phenotype, because *Tfam^{EKO}* mice (Baris et al., 2011), which

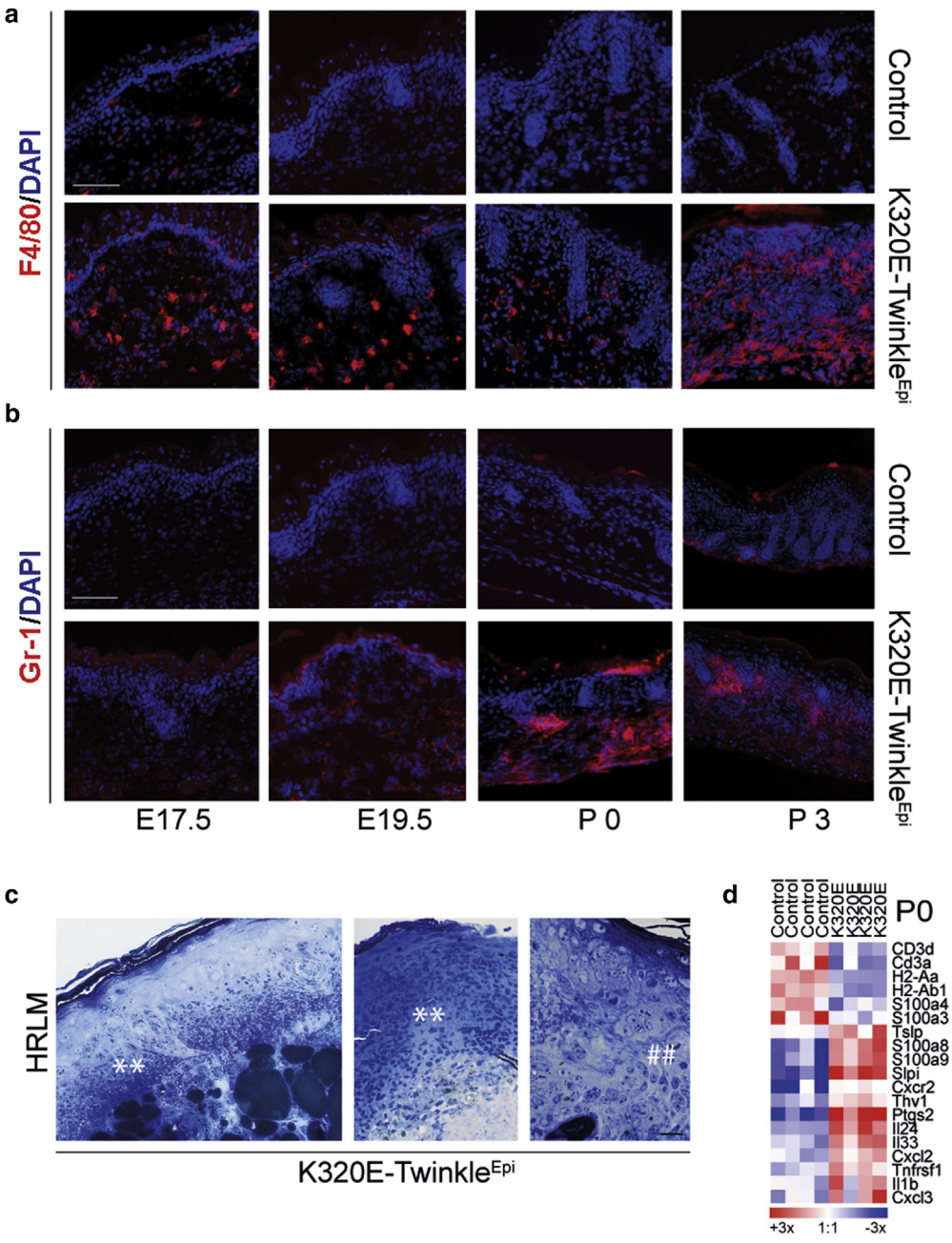

Figure 4. Infiltration of immune cells in the skin of K320E-Twinkle^{Epi} mice. (**a**) Massive infiltrates of macrophages in mutant skin. Red indicates F4/80; blue indicates DAPI. Scale bars = 100 μm. (**b**) Massive infiltrates of neutrophil granulocytes in the mutant skin. Red indicates Gr1; blue indicates DAPI. Scale bar = 100 μm. (**c**) High resolution light microscopy showed the highly granular dermis (**) with a high amount of inflammatory cells, mainly neutrophils (##). Scale bar = 20 μm. (**d**) This inflammation is also reflected by the increased expression of different cytokines and mediators of the immune response at birth in K320E-Twinkle^{Epi} mice. E, embryonic day; HRLM, high-resolution light microscopy; P, postnatal day.

also have dramatically reduced mtDNA copy numbers, do not show skin inflammation (see Supplementary Figure S5b). MtDNA deletions in K320E-Twinkle^{Epi} mice could be detected only at very low amounts, thus arguing against them being the driving force for the observed inflammatory response. Nevertheless, the transient delay in barrier closure at the ventral skin might be involved, because inflammation was localized at the same region and was not detected in the back skin. However, this delay is clearly not sufficient to cause the phenotype, because *Tfam*^{EKO} mice also show a transient delay in barrier closure (see Supplementary Figure S5a). Thus, we postulate that cell-intrinsic mechanisms, induced by the imbalanced RC in K320E-Twinkle^{Epi} mice, cause a unique proinflammatory environment in keratinocytes in utero, which is absent in *Tfam*^{EKO} mice with a completely absent RC in the epidermis.

The response in K320E-Twinkle^{Epi} mice was very similar to the psoriasis-like skin inflammation with scaly plaques, acanthosis, hyperkeratosis, and mixed inflammatory infiltrates reported in mice with epidermis-specific inhibition of NF-κB (Kumari et al., 2013). The up-regulation of several proinflammatory cytokines also reflects, albeit only partially, the situation in this model. In particular, the increased expression of the tumor necrosis factor receptor 1A (Figure 4d, and see Supplementary Table S1) may sensitize keratinocytes to tumor necrosis factor, which then releases IL-24 and other factors, consequently attracting macrophages and granulocytes. Despite these clear similarities, we also noticed major differences with the model described by Pasparakis and colleagues (Kumari et al., 2013). Increased expression of IL-33 (+2.0) was seen in our mice (Figure 4d, and see Supplementary Table S1), which has been shown to

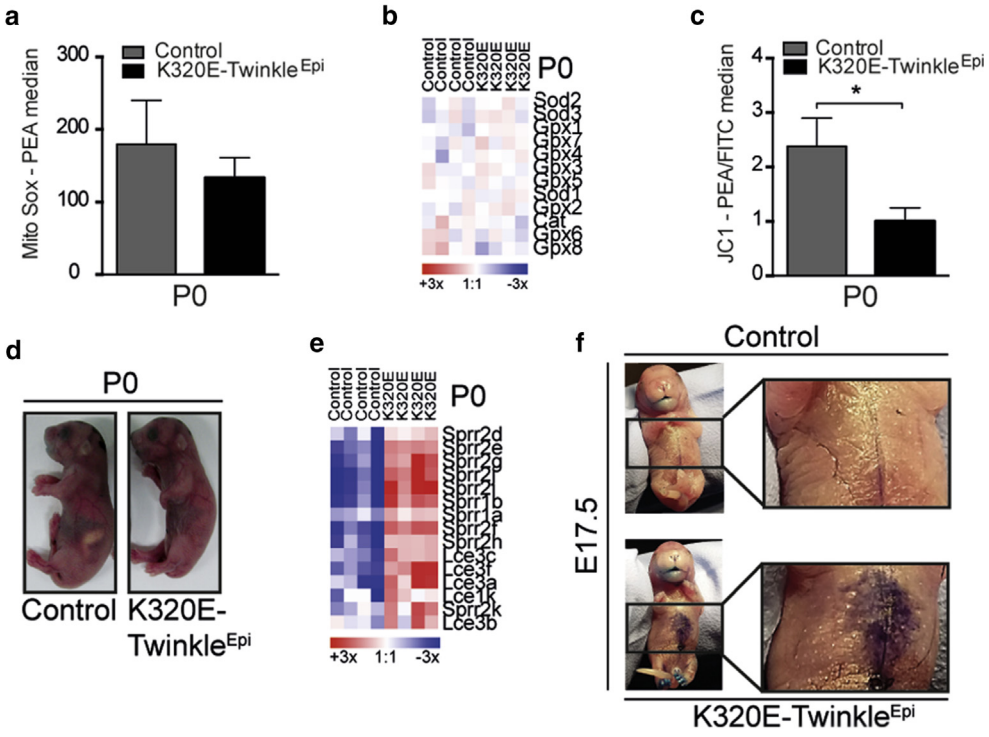

Figure 5. Delayed barrier formation in K320E-Twinkle^{Epi} mice. (**a**) No obvious changes in the production of superoxide in isolated keratinocytes could be detected. n = 5; mean ± standard deviation. (**b**) No differences in the expression of genes involved in antioxidant defense. (**c**) Significant decrease of the inner mitochondrial membrane potential in isolated keratinocytes at birth. n = 5, mean ± standard deviation. *$P < 0.05$). (**d**) Skin barrier function is normal at birth, as shown by toluidine blue assay. (**e**) However, numerous genes encoding small prolin-rich proteins and late cornified envelope proteins have an increased expression. (**f**) This results from a transient delay in barrier closure in utero, as seen by toluidine blue dye penetration at the ventral region of E17.5 K320E-Twinkle^{Epi} embryos. E, embryonic day; P, postnatal day. PEA, phycoerythrin-area.

be an important chemoattractant for neutrophils (Hueber et al., 2011), in accordance with the massive accumulation of neutrophil plaques observed at birth (Figure 4b). These may be mediated by the increased expression of chemokines of the CXCL-family CXCL2 (+1.6) and CXCL3 (+1.8) (Figure 4d, and see Supplementary Table S1). These cytokines may be also triggered by the increased expression of two proteins of the EF hand-type Ca-binding S100 protein family, S100A8 (+3.3) and S100A9 (+2.9) (Nukui et al., 2008), which were also significantly induced in our mutant mice, in addition to TSLP (+1.6), also involved in immune cell attraction (Bjerkan et al., 2016). On the other hand, expression of IL-6 and IL-19, granulocyte macrophage colony stimulation factor (GM-SCF), and chemokines of the CCL family, which were strongly induced after NF-κB inhibition in mice and in human psoriatic epidermis (Kumari et al., 2013), was unchanged. Other genes significantly induced include *Slpi* (+5.4), an antibacterial peptide, and *Ptgs* encoding COX-2 (+5.5), a major mediator of inflammation. In summary, the mitochondrial defect we have induced by our genetic approach leads to a new expression pattern of proinflammatory cytokines and chemokines and ultimately to a phenotype reminiscent of psoriatic skin (Kumari et al., 2013).

The cell intrinsic factors causing these downstream effects are unknown. Mitochondrial damage has been repeatedly postulated to activate the NLRP3 inflammasome by increased ROS production (Heid et al., 2013), by presentation of the inner membrane lipid cardiolipin to the inflammasome (Iyer et al., 2013), or by the presence of oxidized mtDNA in the cytosol (Shimada et al., 2012). Activation of the NLRP3 inflammasome inevitably leads to increased release of IL-1β (reviewed in Gurung et al., 2015). Although a 1.6-fold increase in its mRNA expression could be detected (Figure 4d, and see Supplementary Table S1), isolated keratinocytes did not release IL-1β into the medium, neither from control nor from mutant cells (data not shown, detection limit of ELISA = 1.9 pg/ml). Therefore, we conclude that the NLRP3 inflammasome is not activated by the mitochondrial defect induced in our mice. Also, ROS levels were similar between mutant and control mice (Figure 5b), and there was no indication for an activation of an antioxidant response (Figure 5b), which coincides with the fact that the expression of members of the NF-κB pathway and downstream genes (KEGG mmu04064), also reacting to cellular ROS, was not affected.

The striking difference between K320E-Twinkle^{Epi} mice and *Tfam*^{EKO} mice, which never showed inflammation, may help identify the initiating cell-intrinsic mechanisms causing activation of proinflammatory genes in the presence of a misassembled RC. An obvious candidate could be mtDNA-encoded RNAs released by damaged mitochondria, which still may contain mtDNA at low levels. Those RNAs significantly differ from their nuclear encoded counterparts because of the absence of a 5′ cap structure in mRNAs and divergent posttranscriptional modifications of transfer RNAs and thus may be recognized as viral RNAs in the cytosol. However, such molecules inevitably activate the RIG-1−like receptors and finally activate an IFN-1β response (Loo and Gale, 2011), for which, again, we have no evidence.

Finally, a unique property of proteins encoded by mtDNA is N-formyl-methionine at the N-terminus. Because TFAM is necessary for both mtDNA replication and transcription, the synthesis of mtRNAs and, consequently, of mtDNA-encoded proteins will terminate soon after inactivation of its gene by Cre-recombinase at E14.5. Indeed, we did not detect any RC complexes that contained mtDNA-encoded subunits at birth in *Tfam*^{EKO} mice (see Supplementary Figure S1b), whereas

complex I and III, but not IV, were still present in K320E-Twinkle^{Epi} mice because of ongoing transcription even at low mtDNA copy numbers. We have shown previously that RC proteins are unstable when not properly assembled into supercomplexes and are consequently rapidly degraded (Hornig-Do et al., 2012). Therefore, we propose that ongoing synthesis but rapid degradation of RC proteins will lead to the accumulation of N-formylated peptides, which stimulate the observed immune response. N-formylated peptides have been postulated to act as mitochondrial damage-associated molecular patterns (Galluzzi et al., 2012) and can activate polymorphonuclear neutrophils; however, this was shown only when they were present in the extracellular space (Zhang et al., 2010). Thus, the presentation and release of N-formylated peptides into the extracellular space or, alternatively, the activation of keratinocyte-intrinsic responses could result in the recruitment of immune cells. However, our attempts to measure N-formylated peptides by mass spectroscopy failed, because these molecules were not detectable at steady state.

In conclusion, our studies on *Tfam*^{EKO} and K320E-Twinkle^{Epi} models show that not only does the functionality of the RC need to be preserved to ensure proper skin homeostasis (Kloepper et al., 2015), but also its integrity, because an imbalanced stoichiometry of the different complexes is sensed as a proinflammatory signal, which in combination with other factors can lead to severe inflammation. Thus, although the short lifespan of K320E-Twinkle^{Epi} mice prevented any aging study, the link we unraveled between an imbalanced RC and inflammation suggests that few skin cells with detrimental levels of mtDNA deletions could indeed be involved in the pathogenesis of subclinical chronic inflammation.

MATERIALS AND METHODS

Animals

All animal studies were approved by the animal care committee of the University of Cologne and local government authorities (Bezirksregierung Köln; Landesamt für Natur, Umwelt und Verbraucherschutz [LANUV], Recklinghausen).

Generation of *Tfam*^{EKO} and K320E-*Twinkle*^{Epi} mice

The generation of *Tfam*^{EKO} mice was previously described (Baris et al., 2011). K320E-Twinkle^{Epi} mice were generated by crossing keratin 14-Cre mice (Hafner et al., 2004) with R26-K320E-Twinkle$^{loxP/+}$ mice (Baris et al., 2015). Cre recombination leads to the expression of both K320E-TWINKLE and GFP in the epidermis. Littermates with the genotype *Tfam*$^{loxP/loxP}$ and R26-K320E-Twinkle$^{loxP/+}$ were used as controls for *Tfam*^{EKO} and K320E-Twinkle^{Epi} mice, respectively. The specificity of cre recombination was checked by PCR using total tissue DNA extracted with the DNeasy Blood & Tissue Kit (Qiagen, Hilden, Germany).

Blood glucose and lactate levels measurement

Blood glucose and lactate levels were measured on freshly sampled blood using the GlucoMen LX (Menarini Diagnostics, Winnersh-Wokingham, UK) and the Accutrend Plus (Roche Diagnostics, Basel, Switzerland) devices, respectively.

Tissue collection

Back and ventral skin samples from mice at various ages (postnatal days 0–8) were either snap-frozen, embedded in optimal cutting temperature compound (Tissue-Tek; Sakura, Alphen aan den Rijn, The Netherlands) or fixed in 4% paraformaldehyde for subsequent paraffin embedding. Epidermal sheets were prepared as previously described (Baris et al., 2011).

Quantification of mtDNA copy number and mtDNA deletions

Total DNA was extracted with the DNeasy Blood & Tissue Kit (Qiagen, Hilden, Germany). Presence of mtDNA deletions was investigated using a nested long-range PCR protocol to amplify mtDNA major arc (11 kb). Mitochondrial DNA copy numbers were measured as previously described (Neuhaus et al., 2017). Primer sequences and PCR conditions are available upon request.

Immunoblotting

Epidermal protein extracts were prepared as previously described (Baris et al., 2011). Western blot experiments were carried out using primary antibodies against NDUFB8, SDHB, UQCR2, MTCO1, and ATP5A as index subunits for the RC complexes (MitoSciences, Eugene, OR). Signals were detected using the enhanced chemiluminescence Western blotting detection reagent ECL (Perkin Elmer, Walthan, MA).

COX/succinate dehydrogenase staining

Cryosections of back skin (10 μm) were sequentially stained for COX and succinate dehydrogenase activity as previously described (Sciacco and Bonilla, 1996). In this assay, a significant drop in mtDNA encoded subunits is shown when brown precipitates are absent, so that blue staining becomes apparent.

Histology

Hematoxylin/eosin was used to assess skin morphology. Staining was performed on deparaffinized sections using a previously described protocol (Baris et al., 2011), with antibodies against β-catenin (BD Transduction Laboratories, San Jose, CA), F4/80 (AbD Serotec, Bio-Rad, Hercules, CA), Gr-1 (BD Pharmingen, San Diego, CA), keratin 14 (Covance, Princeton, JN), keratin 10 (Progen, Heidelberg, Germany), Ki-67 (Abcam, Cambridge, UK), loricrin (Covance, Princeton, NJ), and TOM20 (Santa Cruz Biotechnology, Santa Cruz, CA). The staining for β-catenin (not shown) was used to determine the thickness of the interfollicular epidermis in the samples (ImageJ software, version 1.47, National Institutes of Health, Bethesda, MD).

High-resolution light microscopy

Skin samples were fixed in half-strength Karnovsky's fixative as 3-mm^3 tissue cubes. The tissues were post-fixed in 2% osmium tetroxide and embedded in araldite resin, as described previously (Tobin et al., 1991). Semi-thin sections were stained with toluidine blue/borax for further examination by light microscopy.

Statistics

No statistical method was used to estimate sample size. No randomization or blinding was used in this study. Because of the size of some sample groups ($n = 3–5$), normality of the distribution could not be assessed. Therefore, statistical analysis was performed with the assumption that all data were normally distributed. All data are expressed as mean ± one standard deviation. All comparisons were performed using unpaired Student *t* test with unequal variance. A *P*-value less than 0.05 was regarded as statistically significant.

CONFLICT OF INTEREST

The authors state no conflict of interest.

ACKNOWLEDGMENTS

We thank Maria Bust, Petra Kirschner, Alexander Müller, Kristina Probst, and Annika Schmitz for excellent technical help. This work was funded by grants from the Deutsche Forschungsgemeinschaft (Wi 889/6-3 to RJW, SFB 829 A14 to RJW, Cologne Excellence Cluster on Cellular Stress Responses in Aging-associated Diseases—CECAD to RJW, BR2304/9-1 to BB, and SFB 829 A1, A5, and Z2 to CMN) and the Center of Molecular Medicine Cologne of the Medical Faculty (CMMC, to RJW).

SUPPLEMENTARY MATERIAL

Supplementary material is linked to the online version of the paper at www.jidonline.org, and at https://doi.org/10.1016/j.jid.2017.08.019.

REFERENCES

Baris OR, Ederer S, Neuhaus JF, von Kleist-Retzow JC, Wunderlich CM, Pal M, et al. Mosaic deficiency in mitochondrial oxidative metabolism promotes cardiac arrhythmia during aging. Cell Metab 2015;21:667–77.

Baris OR, Klose A, Kloepper JE, Weiland D, Neuhaus JF, Schauen M, et al. The mitochondrial electron transport chain is dispensable for proliferation and differentiation of epidermal progenitor cells. Stem Cells 2011;29:1459–68.

Berneburg M, Grether-Beck S, Kurten V, Ruzicka T, Briviba K, Sies H, et al. Singlet oxygen mediates the UVA-induced generation of the photoaging-associated mitochondrial common deletion. J Biol Chem 1999;274:15345–9.

Birch-Machin MA, Tindall M, Turner R, Haldane F, Rees JL. Mitochondrial DNA deletions in human skin reflect photo- rather than chronologic aging. J Invest Dermatol 1998;110:149–52.

Bjerkan L, Sonesson A, Schenck K. Multiple functions of the new cytokine-based antimicrobial peptide thymic stromal lymphopoietin (TSLP). Pharmaceuticals 2016;9(3):41.

Chen H, Vermulst M, Wang YE, Chomyn A, Prolla TA, McCaffery JM, et al. Mitochondrial fusion is required for mtDNA stability in skeletal muscle and tolerance of mtDNA mutations. Cell 2010;141:280–9.

Dai Y, Zheng K, Clark J, Swerdlow RH, Pulst SM, Sutton JP, et al. Rapamycin drives selection against a pathogenic heteroplasmic mitochondrial DNA mutation. Hum Mol Genet 2014;23:637–47.

Eshaghian A, Vleugels RA, Canter JA, McDonald MA, Stasko T, Sligh JE. Mitochondrial DNA deletions serve as biomarkers of aging in the skin, but are typically absent in nonmelanoma skin cancers. J Invest Dermatol 2006;126:336–44.

Franceschi C, Garagnani P, Vitale G, Capri M, Salvioli S. Inflammaging and 'Garb-aging'. Trends Endocrin Met 2017;28:199–212.

Galluzzi L, Kepp O, Kroemer G. Mitochondria: master regulators of danger signalling. Nat Rev Mol Cell Biol 2012;13:780–8.

Goffart S, Cooper HM, Tyynismaa H, Wanrooij S, Suomalainen A, Spelbrink JN. Twinkle mutations associated with autosomal dominant progressive external ophthalmoplegia lead to impaired helicase function and in vivo mtDNA replication stalling. Hum Mol Genet 2009;18:328–40.

Gurung P, Lukens JR, Kanneganti TD. Mitochondria: diversity in the regulation of the NLRP3 inflammasome. Trends Mol Med 2015;21:193–201.

Hafner M, Wenk J, Nenci A, Pasparakis M, Scharffetter-Kochanek K, Smyth N, et al. Keratin 14 Cre transgenic mice authenticate keratin 14 as an oocyte-expressed protein. Genesis 2004;38:176–81.

Hamanaka RB, Glasauer A, Hoover P, Yang S, Blatt H, Mullen AR, et al. Mitochondrial reactive oxygen species promote epidermal differentiation and hair follicle development. Sci Signal 2013;6(261):ra8.

Heid ME, Keyel PA, Kamga C, Shiva S, Watkins SC, Salter RD. Mitochondrial reactive oxygen species induces NLRP3-dependent lysosomal damage and inflammasome activation. J Immunol 2013;191:5230–8.

Hornig-Do HT, Tatsuta T, Buckermann A, Bust M, Kollberg G, Rotig A, et al. Nonsense mutations in the COX1 subunit impair the stability of respiratory chain complexes rather than their assembly. EMBO J 2012;31:1293–307.

Hudson G, Deschauer M, Busse K, Zierz S, Chinnery PF. Sensory ataxic neuropathy due to a novel C10Orf2 mutation with probable germline mosaicism. Neurology 2005;64:371–3.

Hueber AJ, Alves-Filho JC, Asquith DL, Michels C, Millar NL, Reilly JH, et al. IL-33 induces skin inflammation with mast cell and neutrophil activation. Eur J Immunol 2011;41:2229–37.

Huebner AJ, Dai D, Morasso M, Schmidt EE, Schafer M, Werner S, et al. Amniotic fluid activates the nrf2/keap1 pathway to repair an epidermal barrier defect in utero. Dev Cell 2012;23:1238–46.

Iyer SS, He Q, Janczy JR, Elliott EI, Zhong Z, Olivier AK, et al. Mitochondrial cardiolipin is required for Nlrp3 inflammasome activation. Immunity 2013;39:311–23.

Jurk D, Wilson C, Passos JF, Oakley F, Correia-Melo C, Greaves L, et al. Chronic inflammation induces telomere dysfunction and accelerates ageing in mice. Nat Comm 2014;2:4172.

Kloepper JE, Baris OR, Reuter K, Kobayashi K, Weiland D, Vidali S, et al. Mitochondrial function in murine skin epithelium is crucial for hair follicle morphogenesis and epithelial-mesenchymal interactions. J Invest Dermatol 2015;135:679–89.

Koch PJ, de Viragh PA, Scharer E, Bundman D, Longley MA, Bickenbach J, et al. Lessons from loricrin-deficient mice: compensatory mechanisms maintaining skin barrier function in the absence of a major cornified envelope protein. J Cell Biol 2000;151:389–400.

Krishnan KJ, Harbottle A, Birch-Machin MA. The use of a 3895 bp mitochondrial DNA deletion as a marker for sunlight exposure in human skin. J Invest Dermatol 2004;123:1020–4.

Kumari S, Bonnet MC, Ulvmar MH, Wolk K, Karagianni N, Witte E, et al. Tumor necrosis factor receptor signaling in keratinocytes triggers interleukin-24-dependent psoriasis-like skin inflammation in mice. Immunity 2013;39:899–911.

Larsson NG. Somatic mitochondrial DNA mutations in mammalian aging. Annu Rev Biochem 2010;79:683–706.

Loo YM, Gale M, Jr. Immune signaling by RIG-I-like receptors. Immunity 2011;34:680–92.

Neuhaus JF, Baris OR, Kittelmann A, Becker K, Rothschild MA, Wiesner RJ. Catecholamine metabolism induces mitochondrial DNA deletions and leads to severe adrenal degeneration during aging. Neuroendocrinology 2017;104:72–84.

Nukui T, Ehama R, Sakaguchi M, Sonegawa H, Katagiri C, Hibino T, et al. S100A8/A9, a key mediator for positive feedback growth stimulation of normal human keratinocytes. J Cell Biochem 2008;104:453–64.

Ponnappan S, Ponnappan U. Aging and immune function: molecular mechanisms to interventions. Antioxd Redox Signal 2011;14:1551–85.

Ray AJ, Turner R, Nikaido O, Rees JL, Birch-Machin MA. The spectrum of mitochondrial DNA deletions is a ubiquitous marker of ultraviolet radiation exposure in human skin. J Invest Dermatol 2000;115:674–9.

Rygiel KA, Miller J, Grady JP, Rocha MC, Taylor RW, Turnbull DM. Mitochondrial and inflammatory changes in sporadic inclusion body myositis. Neuropathol Appl Neurobiol 2015;41:288–303.

Sciacco M, Bonilla E. Cytochemistry and immunocytochemistry of mitochondria in tissue sections. Methods Enzymol 1996;264:509–21.

Shimada K, Crother TR, Karlin J, Dagvadorj J, Chiba N, Chen S, et al. Oxidized mitochondrial DNA activates the NLRP3 inflammasome during apoptosis. Immunity 2012;36:401–14.

Spelbrink JN, Li FY, Tiranti V, Nikali K, Yuan QP, Tariq M, et al. Human mitochondrial DNA deletions associated with mutations in the gene encoding Twinkle, a phage T7 gene 4-like protein localized in mitochondria. Nat Genet 2001;28:223–31.

Tobin DJ, Fenton DA, Kendall MD. Cell degeneration in alopecia areata. An ultrastructural study. Am J Dermatopathol 1991;13:248–56.

van der Burgh R, Boes M. Mitochondria in autoinflammation: cause, mediator or bystander? Trends Endocrinol Metab 2015;26:263–71.

Volmering E, Niehusmann P, Peeva V, Grote A, Zsurka G, Altmuller J, et al. Neuropathological signs of inflammation correlate with mitochondrial DNA deletions in mesial temporal lobe epilepsy. Acta Neuropathol 2016;132:277–88.

Zhang Q, Raoof M, Chen Y, Sumi Y, Sursal T, Junger W, et al. Circulating mitochondrial DAMPs cause inflammatory responses to injury. Nature 2010;464(7285):104–7.

Zhuang Y, Lyga J. Inflammaging in skin and other tissues—the roles of complement system and macrophage. Inflamm Allergy Drug Targets 2014;13:153–61.

Zouboulis CC, Makrantonaki E. Clinical aspects and molecular diagnostics of skin aging. Clin Dermatol 2011;29:3–14.